

Lightcurves of Stars & Exoplanets: Estimating Inclination, Obliquity, and Albedo

Nicolas B. Cowan^{1,2}, Pablo A. Fuentes³ and Hal M. Haggard⁴

¹*Center for Interdisciplinary Exploration and Research in Astrophysics (CIERA),*

Northwestern University, 2131 Tech Dr. Evanston, IL 60208, USA (n-cowan@northwestern.edu)

²*Department of Physics and Astronomy, Northwestern University, 2145 Sheridan Rd., F165, Evanston, IL 60208, USA*

³*Department of Astronomy, University of Chile, Camino El Observatorio # 1515, Las Condes, Santiago, Chile*

⁴*Centre de Physique Théorique de Luminy, Campus de Luminy, Case 907 13288 Marseille cedex 9, France*

29 March 2019

ABSTRACT

Exoplanets will remain spatially unresolved for the foreseeable future. It is in principle possible to determine a planet’s brightness markings by analyzing its disk-integrated brightness variations, in either thermal or reflected light. In order to identify the degeneracies inherent in these inverse problems, we develop analytic solutions to the associated forward problems. Our approach is to compute the “harmonic lightcurves” resulting from spherical harmonic maps of intensity or albedo. The convolutions often contain a nullspace: a class of non-zero maps that have no lightcurve signature. We derive harmonic thermal lightcurves for both equatorial and inclined observers. The nullspace for these two situations is significantly different, with odd modes being present in the latter case, but not the former. We therefore suggest that the Fourier spectrum of a thermal lightcurve is sufficient to determine the orbital inclination of non-transiting short-period planets, the rotational inclination of stars and brown dwarfs, and the obliquity of directly imaged planets. In the best-case scenario of a nearly edge-on rotator, factor-of-two measurements of the amplitudes of odd modes in the thermal lightcurve provide an inclination estimate good to a few degrees. In general, however, inclination estimates will remain qualitative until detailed hydrodynamic simulations and/or occultation maps can be used as a calibrator. We further derive harmonic reflected lightcurves for tidally-locked planets; these are higher-order versions of the well-known Lambert phase curve. We show that a non-uniform diffusely-reflecting planet with a precisely Lambertian phase curve may have planetary and Bond albedos significantly different from that inferred if the planet is assumed to be uniform. Lastly, we provide low-order analytic expressions for harmonic lightcurves that can be used for fitting observed photometry; as a general rule, edge-on solutions cannot simply be scaled by $\sin i$ to mimic inclined lightcurves.

1 INTRODUCTION

1.1 Motivation

Extrasolar planets are sufficiently small and distant that they will remain spatially unresolved for the foreseeable future. It is nonetheless possible to infer spatial inhomogeneities on these bodies through a) occultations, as when a planet passes behind its host star (Majeau et al. 2012; de Wit et al. 2012), or b) orbital and rotational motion (e.g., Knutson et al. 2007; Cowan et al. 2009). At thermal wavelengths, such maps probe the magnetic fields of stars, large-scale atmospheric circulation of sub-stellar objects, as well as thermal inertia and albedo inhomogeneities of airless bodies. Exo-cartography with reflected light, on the other hand, constrains the albedo markings of planets.

In the current study we consider photometric variability due to rotational and orbital motion, i.e. method b). We seek an analytic solution to the convolution relating intrinsic spatial inhomogeneities of the planet to time-variations in disk-integrated brightness measured by a distant observer. In particular, we consider changes in disk-integrated thermal flux due to spatial inhomogeneities in thermal emission, and variations in disk-integrated reflectance due to spatial inhomogeneities in albedo.

Russell (1906) showed how time-resolved photometry of reflected light constrains the albedo markings, shape, and rotational orientation of minor Solar System bodies observed near opposition (full phase). In addition to revealing brightness markings on stars and planets, rotational and orbital phase variations likewise have the potential to constrain rotational

and orbital inclination. Possible applications include: the thermal phase variations of non-transiting hot Jupiters might hint at their orbital inclination, breaking the $M \sin i$ degeneracy and allowing for improved mass estimates; the rotational phase variations of a transiting planet's host star may be sufficient to infer its rotational inclination (a.k.a. stellar obliquity), a useful discriminator between planet migration scenarios (Winn et al. 2005); the rotational photometric variations of a directly-imaged planet might encode information about its rotational inclination which —when combined with the astrometrically inferred orbital inclination— provides an estimate of planetary obliquity, telling us about planet formation (Tremaine 1991).

1.2 Forward vs. Inverse Problem

Inferring the properties of a star or planet based on its disk-integrated brightness is an *inverse problem*, as opposed to the *forward problem* of predicting the photometry of an object based on its properties. There are two broad approaches to solving this inverse problem: 1) develop a forward model with unknown parameters, then use a χ^2 -minimizer or Markov Chain Monte Carlo (MCMC) to solve for the parameters, or 2) approximate the forward problem by an analytic transformation that has an explicit inverse. The advantages of the former method are that the forward model may be arbitrarily sophisticated, and parameter uncertainties can be readily estimated; the advantages of the latter are speed and the ability to explicitly identify degeneracies. A typical compromise is to adopt a simple linear approximation to the forward model, but use a MCMC or similar routine to obtain best-fit parameters and uncertainties.

In this work we seek an analytic solution to the forward problem that would lend itself to an analytic inverse. This entails determining the basis lightcurves for a set of complete and orthonormal basis maps. We approximate the forward problem as linear in the unknown planet map, $M(\theta, \phi)$:

$$F(t) = \oint K(\theta, \phi, t)M(\theta, \phi)d\Omega, \quad (1)$$

where $F(t)$ is the observed flux, $K(\theta, \phi, t)$ is the kernel, θ and ϕ are planetary co-latitude and longitude, respectively. The inverse problem, solving for M given K and F , is a Fredholm integral equation of the first kind and is non-trivial (Aster, Borchers & Thurber 2013).

As we will see below, the kernel is non-negative and unimodal. It is therefore tempting to think of (1) as a convolution, and the inverse problem as a deconvolution. For thermal lightcurves, K has a fixed shape and this description is formally correct; in other cases it is merely a useful analogy.

If the orientation of the planet or star is not known *a priori*, then the problem can be expressed as

$$F(t) = \oint K(\mathbb{G}, \theta, \phi, t)M(\theta, \phi)d\Omega, \quad (2)$$

where \mathbb{G} represents the unknown geometry (inclination or obliquity). The object is then to solve for \mathbb{G} and $M(\theta, \phi)$ knowing F and *the form* of K . It has been demonstrated in numerical experiments, for example, that one can simultaneously constrain a planet's two-dimensional albedo map, obliquity and obliquity phase (Kawahara & Fujii 2010, 2011; Fujii & Kawahara 2012).

In the current work we seek an analytic solution to the forward problem, and hence a rapid and elegant approach to the inverse problem. Whenever possible, we solve the integrals analytically by hand and/or with *Mathematica*. When symbolic solutions are too messy to have intuitive value, we use *IDL* to compute and plot numerical integrals. In §2 we describe our chosen basis maps and lightcurves. We tackle thermal lightcurves in §3 before addressing the more complex case of reflected lightcurves in §4. In both of those sections we begin by describing our model assumptions for the forward problem, then present solutions to special cases before moving on to the general solution. Some of the mathematical details are relegated to the Appendix in order to keep the main body of the manuscript accessible. We discuss possible applications of this work in §5.

2 HARMONIC LIGHTCURVES

In order to develop an analytic solution to (1), it is necessary to express the planetary map analytically. In general this is done by decomposing M using an orthonormal basis. The obvious basis maps for a spherical planet are spherical harmonics. Any continuous, static albedo map, $M(\theta, \phi)$, may be decomposed as

$$M(\theta, \phi) = \sum_{l=0}^{\infty} \sum_{m=-l}^l C_l^m Y_l^m(\theta, \phi), \quad (3) \quad C_l^m = \frac{1}{4\pi} \oint M(\theta, \phi) Y_l^m(\theta, \phi) d\Omega. \quad (4)$$

The real spherical harmonics are given by

$$Y_l^m(\theta, \phi) = \begin{cases} N_l^m P_{lm}(\cos \theta) \cos(m\phi) & \text{if } m \geq 0 \\ N_l^{|m|} P_{l|m|}(\cos \theta) \sin(|m|\phi) & \text{if } m < 0, \end{cases} \quad (5)$$

where P_{lm} is the associated Legendre polynomial without the Condon-Shortley phase, $(-1)^m$.

We adopt the geodesy normalization (unit power) for real spherical harmonics,

$$N_l^m = \begin{cases} 1 & \text{if } l = 0 \\ \sqrt{\frac{2(2l+1)(l-m)!}{(l+m)!}} & \text{if } l > 0, \end{cases} \quad (6) \quad \frac{1}{4\pi} \oint Y_l^m(\theta, \phi) Y_l^{\mu}(\theta, \phi) d\Omega = \delta_{l\lambda} \delta_{m\mu}. \quad (7)$$

The goal of this project is to determine the lightcurve signatures of spherical harmonics, or *harmonic lightcurves*,

$$F_l^m(t) = \oint K(\theta, \phi, t) Y_l^m(\theta, \phi) d\Omega. \quad (8)$$

It is perfectly equivalent to think of this as decomposing the kernel into spherical harmonics.

Since (1) is linear in M , the lightcurve for an arbitrary albedo map is simply

$$F(t) = \sum_{l=0}^{\infty} \sum_{m=-l}^l C_l^m F_l^m(t). \quad (9)$$

The dream of exo-cartography is to take the inner product of an observed lightcurve with known harmonic lightcurves to determine map coefficients:

$$C_l^m = \frac{1}{P} \int_0^P F_l^m(t) F(t) dt, \quad (10)$$

where P is the period of the lightcurve. A map of the planet could then be reconstructed using (3). In this paper we will encounter two problems with this strategy. First of all, some of the harmonic lightcurves are flat lines ($F \equiv 0$). In other words, the transformation has a nullspace.¹ Secondly, even non-zero harmonic lightcurves are sometimes proportional to each other. This is not surprising, since linear transformations need not preserve angles: planetary maps that are orthogonal are not necessarily transformed to lightcurves that are orthogonal. The bottom line is that exo-cartography suffers from formal degeneracies, even in the limit of perfect observations.

3 THERMAL LIGHTCURVES

3.1 Model Formalism

We assume a static brightness map, diffuse thermal emission, and neglect limb-darkening. The requirement of a static map depends on context. For mapping star spots or patchy clouds on a brown dwarf, the rotation rate is the relevant timescale. When mapping the diurnal heating pattern of a planet, on the other hand, one requires stability on the orbital period (for more about the various sources of planetary thermal variability see Cowan et al. 2012c).

The flux, F , in this case is the disk-integrated thermal flux from the planet. The kernel is proportional to the visibility of a given region of the planet at time t : $K(\theta, \phi, t) = \frac{1}{\pi} V(\theta, \phi, t)$, where the visibility, V , is unity at the sub-observer location, drops as the cosine of the angle from the sub-observer location, γ_o , and is zero on the far side of the planet:

$$V(\theta, \phi, t) = \max[\cos \gamma_o, 0] = \max[\sin \theta \sin \theta_o \cos(\phi - \phi_o) + \cos \theta \cos \theta_o, 0], \quad (11)$$

where θ_o and ϕ_o are the sub-observer latitude and longitude, respectively. The piece-wise defined nature of the kernel leads to much of the difficulty in solving the forward problem analytically.

The entire time-dependence of the forward problem comes in through the sub-observer position. In the absence of precession, the sub-observer latitude is constant, $\theta_o(t) = \theta_o$. The sub-observer longitude decreases linearly with time (we define longitude increasing to the East, with the planet rotating from West to East): $\phi_o(t) = \phi_o(0) - \omega_{\text{rot}} t$, where ω_{rot} is the rotational angular frequency *in an inertial frame* (e.g., $\omega_{\text{rot}} = 2\pi/23.93 \text{ hr}^{-1}$ for Earth).

Given a thermal map of the planet, the harmonic lightcurves are given by

$$F_l^m(t) = \frac{1}{\pi} \oint V(\theta, \phi, t) Y_l^m(\theta, \phi) d\Omega. \quad (12)$$

Integrating the piece-wise defined kernel over the entire sphere is equivalent to integrating the non-zero part of the kernel, $K_{\text{nz}}(\theta, \phi, t) = \frac{1}{\pi} (\sin \theta \sin \theta_o \cos(\phi - \phi_o) + \cos \theta \cos \theta_o)$, over the visible hemisphere. The limits of integration are then defined by the limb, the locus of points with $\gamma_o = \pi/2$. From (11), the limb satisfies:

$$\tan \theta_{\text{limb}} = \frac{-1}{\tan \theta_o \cos(\phi - \phi_o)}, \quad (13)$$

as shown in Figure 1.

For a planet viewed equator-on ($\theta_o = \pi/2$) the kernel simplifies to: $K_{\text{nz}}(\theta, \phi, t) = \frac{1}{\pi} \sin \theta \cos(\phi - \phi_o)$.

¹ The term “kernel” is often used interchangeably with “nullspace” in mathematical physics, but we eschew that terminology here because “kernel” already has a central role in convolutions.

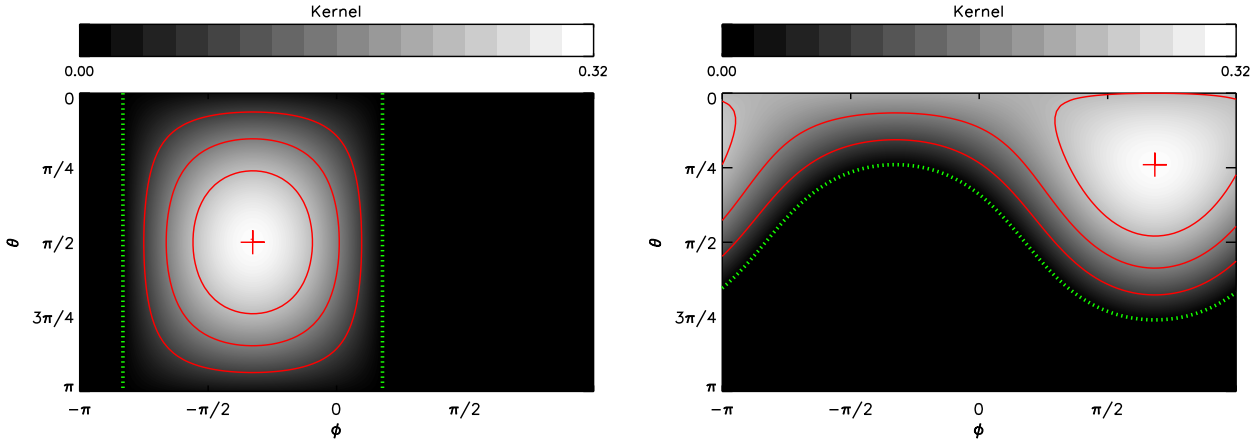


Figure 1. The visibility (red contours) of a planet seen by an equatorial (left) or northern observer (right). The gray-scale shows the kernel of the convolution, which in this case is simply the rescaled visibility. The sub-observer location is denoted by a red cross. The limb is shown in each case with green dotted lines. For either viewing geometry, the limb is a great circle and the non-zero portion of the kernel is a hemisphere.

3.2 Equator-On Thermal Lightcurve

We first consider a planet viewed equator-on (left panel of Figure 1), which allows us to separate (12) into two single integrals:

$$F_l^m(t) = \frac{N_l^m}{\pi} \int_{-1}^1 \sqrt{1-x^2} P_{lm}(x) dx \int_{\phi_o - \frac{\pi}{2}}^{\phi_o + \frac{\pi}{2}} \cos(\phi - \phi_o) \cos(m\phi) d\phi, \quad (14)$$

where we have made the change of coordinates $x = \cos\theta$. Note that we have given the example for a cosine Y_l^m ($m \geq 0$), but the sine instance ($m < 0$) can be trivially obtained by replacing $m \rightarrow |m|$ and $\cos(m\phi) \rightarrow \sin(|m|\phi)$.

The time-dependence can be factored out of the integral by making the change of variables $\Phi = \phi - \phi_o$, using a trigonometric identity, and noting that one of the two resulting integrals is zero (or simply using complex exponentials):

$$F_l^m(t) = \frac{N_l^m}{\pi} \cos(m\phi_o) \int_{-1}^1 \sqrt{1-x^2} P_{lm}(x) dx \int_{-\frac{\pi}{2}}^{\frac{\pi}{2}} \cos(\Phi) \cos(m\Phi) d\Phi, \quad (15)$$

where the product of integrals is now solely a function of l and m . Recalling that $\phi_o \propto t$, Fourier analysis implies $\int_0^P F_l^m F_\lambda^\mu dt = 0$ for $\mu \neq m$, and justifies the use of sinusoidal basis maps by Cowan & Agol (2008).

The integral of the Associate Legendre Polynomial is simplified by using a recurrence relation, then solved directly following Jepsen et al. (1955), as described in Appendix A:

$$\int_{-1}^1 \sqrt{1-x^2} P_{lm}(x) dx = \frac{1}{(2l+1)} [R_{l+1}^{m+1} - R_{l-1}^{m+1}]. \quad (16)$$

The integral of an associated Legendre polynomial over the interval $x \in [-1, 1]$, represented here as R_l^m , depends on the parity of the spherical harmonic. If l and m are even, then $l-1$, $l+1$, and $m+1$ are odd; if l and m are odd, then $l-1$, $l+1$, and $m+1$ are even; if $l+m$ is odd, then so are $(l-1) + (m+1)$ and $(l+1) + (m+1)$. Lastly, $R_{l-1}^{m+1} = R_{l+1}^{m+1}$ for odd $l > 1$, producing a nullspace, $F_l^m = 0$.

The Φ -integral yields:

$$\int_{-\frac{\pi}{2}}^{\frac{\pi}{2}} \cos\Phi \cos(m\Phi) d\Phi = \begin{cases} \frac{\pi}{2} & \text{if } |m| = 1 \\ \frac{2}{1-m^2} \cos\left(\frac{m\pi}{2}\right) & \text{if } |m| \neq 1, \end{cases} \quad (17)$$

which recovers the Cowan & Agol (2008) result of zero phase signature for odd $|m| > 1$, since $\cos\left(\frac{m\pi}{2}\right)$ is zero in those cases. Physically, the brightness inhomogeneities cancel each other in the disk-integrated case. Mathematically, Y_l^m with odd $|m| > 1$ are in the nullspace of the convolution.

Combining (16) and (17) yields the full solution,

$$F_l^m(t) = \begin{cases} 1 & \text{if } l = 0 \\ \frac{2}{\sqrt{3}} \cos\phi_o & \text{if } l = 1 \text{ and } m = 1 \\ \frac{2(-1)^{m/2}}{\pi(1-m^2)} \sqrt{\frac{2(l-m)!}{(2l+1)(l+m)!}} [R_{l+1}^{m+1}(\text{odd}) - R_{l-1}^{m+1}(\text{odd})] \cos(m\phi_o) & \text{if } l \text{ and } m \text{ are even} \\ 0 & \text{otherwise,} \end{cases} \quad (18)$$

where $R_l^m(\text{odd})$ is given in Appendix A. The nullspace is the union of odd $m > 1$ (Φ -integral goes to zero) and odd $l > 1$ (x -integral goes to zero).

The first few non-zero harmonic lightcurves are:

$$F_0^0(t) = 1 \quad (19)$$

$$F_1^1(t) = \frac{2}{\sqrt{3}} \cos \phi_o \quad (20)$$

$$F_2^0(t) = -\frac{\sqrt{10}}{8} \quad (21)$$

$$F_2^2(t) = \frac{\sqrt{15}}{8} \cos(2\phi_o) \quad (22)$$

$$F_4^0(t) = -\frac{3\sqrt{2}}{64} \quad (23)$$

$$F_4^2(t) = \frac{\sqrt{5}}{32} \cos(2\phi_o) \quad (24)$$

$$F_4^4(t) = -\frac{\sqrt{35}}{64} \cos(4\phi_o), \quad (25)$$

where again we stress that the sine harmonic lightcurves ($m < 0$) can be trivially obtained by replacing $m \rightarrow |m|$ and $\cos \rightarrow \sin$.

3.3 Inclined Thermal Lightcurve

For a general (non-equatorial) observer, one of the poles is visible and the other is invisible, rather than both being on the limb (right panel of Figure 1). The ϕ -integral therefore runs from 0 to 2π , while the θ -integral runs from 0 to $\theta_{\text{limb}}(\phi)$ if the north pole is visible, or from $\theta_{\text{limb}}(\phi)$ to π if the south pole is visible. With no loss of generality we consider a northern observer:

$$F_l^m(t) = \frac{N_l^m}{\pi} \left[\sin \theta_o \int_0^{2\pi} \cos(\phi - \phi_o) \cos(m\phi) \int_{x_{\text{limb}}}^1 \sqrt{1-x^2} P_{lm}(x) dx d\phi + \cos \theta_o \int_0^{2\pi} \cos(m\phi) \int_{x_{\text{limb}}}^1 x P_{lm}(x) dx d\phi \right], \quad (26)$$

where $x_{\text{limb}} = \cos \theta_{\text{limb}}$.

As with the equatorial geometry, the time-dependence may be factored out of the integral using complex exponentials:

$$F_l^m(t) = \frac{N_l^m}{\pi} \cos(m\phi_o) \left[\sin \theta_o \int_0^{2\pi} \cos \Phi \cos(m\Phi) \int_{x_{\text{limb}}}^1 \sqrt{1-x^2} P_{lm}(x) dx d\Phi + \cos \theta_o \int_0^{2\pi} \cos(m\Phi) \int_{x_{\text{limb}}}^1 x P_{lm}(x) dx d\Phi \right], \quad (27)$$

where (13) dictates that

$$x_{\text{limb}} = \frac{-\tan \theta_o \cos \Phi}{\sqrt{1 + \tan^2 \theta_o \cos^2 \Phi}}. \quad (28)$$

Since x_{limb} is a function of Φ , we cannot separate the x and Φ integrals as in the equatorial case. We instead denote the two double integrals as

$$A_l^m(\theta_o) = \int_0^{2\pi} \cos \Phi \cos(m\Phi) \int_{x_{\text{limb}}}^1 \sqrt{1-x^2} P_{lm}(x) dx d\Phi, \quad (29)$$

$$B_l^m(\theta_o) = \int_0^{2\pi} \cos(m\Phi) \int_{x_{\text{limb}}}^1 x P_{lm}(x) dx d\Phi. \quad (30)$$

Numerically, we find that $A = B = 0$ if and only if l is odd and greater than 1, therefore all thermal harmonic light curves are zero for odd $l > 1$ (we demonstrate this analytically in Appendix B). The nullspace for an inclined geometry is therefore more limited than the equator-on case: there are non-zero harmonic lightcurves with odd $m > 1$ (provided that l is even, e.g. Y_4^3 shown in Figure 2).

As with the equatorial case, one can use recurrence relations to express the x -integrals in terms of sums of simple integrals of $P_l^m(x)$. But while there are recurrence relations for the indefinite integral $\int P_l^m(x) dx$ (DiDonato 1982), we were unable to develop such a relation for the harmonic lightcurves, $F_l^m(t)$. Instead, we use the brute force approach of substituting specific $P_l^m(x)$ into (27) and analytically solving the double integral.

We first solve the indefinite integral over x , which we evaluate at the limits of integration. The resulting integrands for the Φ -integrals include trigonometric functions with singularities. Since the sign of these functions can change on either side of the singularities, the integral over Φ exhibits unphysical jumps.² Fortunately, the jumps occur at predictable fractions of π , and their amplitude is a tractable function of θ_o , so the definite integral can be manually corrected. The resulting low-order non-zero harmonic lightcurves are:

² Although these jumps are undesirable, the derivative of the resulting curve is smooth, so *Mathematica* is indeed returning a valid anti-derivative.

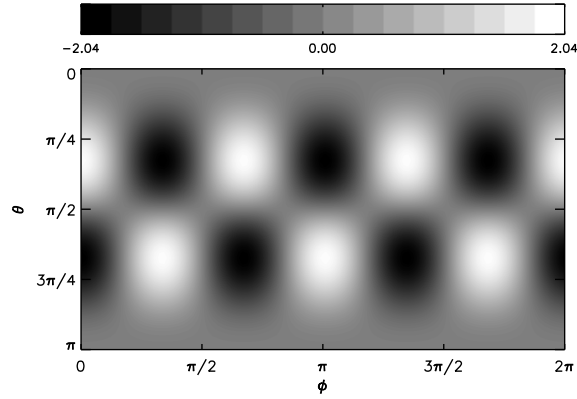


Figure 2. The Y_4^3 brightness map is in the nullspace of the edge-on thermal lightcurve, but not of the inclined lightcurve. It is the lowest-order map that can produce power at odd $m > 1$ in a thermal lightcurve.

$$F_0^0 = 1 \quad (31)$$

$$F_1^0 = \frac{2\sqrt{6}}{3} \cos \theta_o \quad (32)$$

$$F_1^1 = \frac{2}{\sqrt{3}} \sin \theta_o \cos \phi_o \quad (33)$$

$$F_2^0 = \frac{\sqrt{10}}{8} (3 \cos^2 \theta_o - 1) \quad (34)$$

$$F_2^1 = \frac{3}{4} \sqrt{\frac{5}{3}} \sin \theta_o \cos \theta_o \cos \phi_o \quad (35)$$

$$F_2^2 = \frac{\sqrt{15}}{8} \sin^2 \theta_o \cos(2\phi_o) \quad (36)$$

$$F_4^0 = \frac{-\sqrt{2}}{512} (9 + 20 \cos(2\theta_o) + 35 \cos(4\theta_o)) \quad (37)$$

$$F_4^1 = \frac{5}{128\sqrt{10}} (24 \sin \theta_o + 2 \sin 2\theta_o + 7 \sin 4\theta_o) \cos \phi_o \quad (38)$$

$$F_4^2 = \frac{-\sqrt{5}}{64} (5 + 7 \cos 2\theta_o) \sin^2 \theta_o \cos(2\phi_o) \quad (39)$$

$$F_4^3 = \frac{35}{16\sqrt{70}} \cos \theta_o \sin^3 \theta_o \cos(3\phi_o) \quad (40)$$

$$F_4^4 = \frac{-\sqrt{35}}{64} \sin^4 \theta_o \cos(4\phi_o). \quad (41)$$

The sine harmonic lightcurves ($m < 0$) can be trivially obtained by the substitution $\cos(m\phi_o) \rightarrow \sin(|m|\phi_o)$.

In Figure 3 we show the amplitude of low-order harmonic lightcurves as a function of sub-observer latitude, θ_o ($\theta_o = 0$ for pole-on or face-on rotation; $\theta_o = \pi/2$ for equator-on or edge-on rotation). The nullspace of the convolution, and more generally its eigenvalues, is a function of θ_o . Obviously a pole-on object exhibits no rotational variability (left side of the plot). Moreover, an object exhibiting power in $m = 3$ is neither pole-on nor equator-on: the amplitude of F_4^3 exhibits a clear peak at $\theta_o = \pi/3$.

Formally, there are an infinite number of harmonic maps that contribute to the lightcurve power at a given m . However, the low-pass nature of the convolution ensures that most of the power at a given m comes from the lowest-order Y_l^m . If the intrinsic power at Y_4^3 was known a priori and there was no other map contributing $m = 3$ power, then one might hope to estimate rotational inclination simply by measuring the $m = 3$ power present in the lightcurve. But there would still be a two-way degeneracy because θ_o is double-valued for a given amplitude (green line in Figure 3).

4 REFLECTED LIGHTCURVES

4.1 Model Formalism

We assume a spherical planet with a static albedo map on a circular orbit. If one is performing rotational mapping (Cowan et al. 2009) then the map only needs to be constant over a single rotation; or equivalently the recovered map is a diurnal average. For rotational+orbital mapping (“spin-orbit tomography;” Fujii & Kawahara 2012), the map is assumed to be static over an entire planetary orbit (e.g., Hasinoff et al. 2011).

The reflection is treated as diffuse (Lambertian). Note, however, that real surfaces can exhibit specular reflection (Williams & Gaidos 2008) and atmospheres can exhibit Rayleigh or Mie scattering (Robinson et al. 2010). The albedo map should be thought of as a top-of-atmosphere planetary albedo.

Albedo, and hence all of the observables, will in general be a function of wavelength, but since we consider only scattered light, there is no mixing of wavelengths. Our results can be generalized to any number of wavebands (Kawahara & Fujii 2011; Fujii & Kawahara 2012) or arbitrary linear combinations of wavebands (Cowan et al. 2009, 2011; Kawahara & Fujii 2010; Cowan & Strait 2013).

For a uniform planet the resulting phase variations under the assumption of diffuse reflection is the well-known Lambert

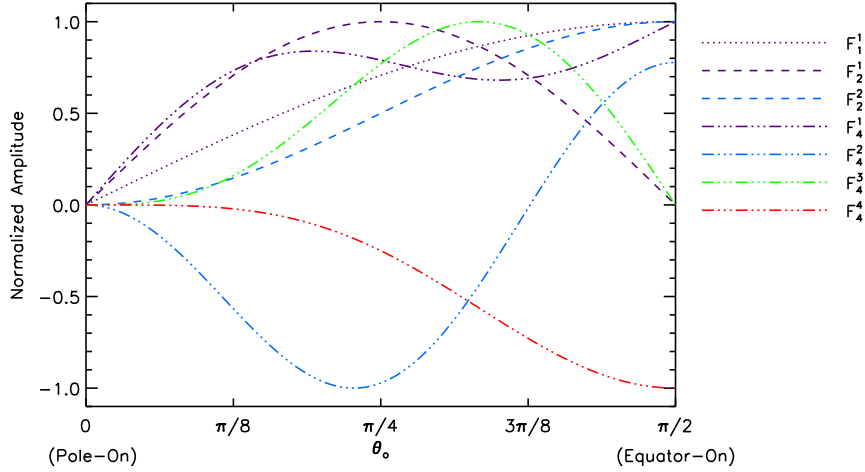


Figure 3. The relative amplitude of harmonic thermal lightcurves as a function of sub-observer latitude (or, equivalently, rotational inclination). Line style denotes l , color denotes m . The nullspace of the convolution is a function of θ_o , allowing for qualitative estimates of rotational inclination based on the Fourier spectrum of observed lightcurves.

phase (Russell 1916). In this section we derive higher moments of the lightcurve. This exercise is complementary to computing the phase variations of uniform but non-Lambertian planets (e.g., Tousey 1957; Madhusudhan & Burrows 2012). Real planets are neither uniform nor Lambertian.

The reflected-light kernel is $K(\theta, \phi, t) = \frac{1}{\pi} V(\theta, \phi, t) I(\theta, \phi, t)$, where the visibility, V is defined as in (11), while the illumination, I , is unity at the sub-stellar location, drops as the cosine of the angle from the sub-stellar location, γ_s , and is zero on the night-side of the planet:

$$I(\theta, \phi, t) = \max[\cos \gamma_s, 0] = \max[\sin \theta \sin \theta_s \cos(\phi - \phi_s) + \cos \theta \cos \theta_s, 0], \quad (42)$$

and θ_s and ϕ_s are the sub-stellar latitude and longitude, respectively. Note that the kernel is proportional to the normalized weight, W , but is not divided by the Lambert phase function (Cowan et al. 2011).

The reflected-light forward problem is therefore:

$$F_l^m(t) = \frac{1}{\pi} \oint V(\theta, \phi, t) I(\theta, \phi, t) Y_l^m(\theta, \phi) d\Omega, \quad (43)$$

where F in this case is the reflectance of the planet, i.e. the planet/star contrast ratio after accounting for the radius and semi-major axis of the planet, which are sometimes not of immediate interest.

Noting that the orbital phase, $\alpha \in [0, \pi]$ ($\alpha = 0$ at full phase; $\alpha = \pi$ at new phase), is simply the angular distance between the sub-observer and sub-stellar points, it may be expressed as

$$\cos \alpha = \sin \theta_o \sin \theta_s \cos(\phi_o - \phi_s) + \cos \theta_o \cos \theta_s = \cos \xi \sin i, \quad (44)$$

where the constant $i \in [0, \pi/2]$ is the orbital inclination with respect to the celestial plane ($i = 0$ for a face-on orbit; $i = \pi/2$ for edge-on), and $\xi = \xi(0) + \omega_{\text{orb}} t$ is the planet's orbital location ($\xi \in [0, 2\pi]$; $\xi = 0$ at superior conjunction; $\xi = \pi$ at inferior conjunction).

As with the thermal emission problem, the crux stems from the piece-wise defined kernel, or equivalently, the limits of integration for the non-zero portion of the kernel. The reflected lightcurve calculation is harder than the thermal lightcurve because the non-zero region of the integral is a lune rather than a hemisphere.

The analytic expressions for the limits of integration allow us to drop the piecewise-defined version of the visibility and illumination functions. If one only considers those regions where both illumination and visibility are greater than zero (ie: those within the limits of integration), then the kernel is:

$$\pi K_{nz}(\theta, \phi, t) = (\sin \theta \sin \theta_o \cos(\phi - \phi_o) + \cos \theta \cos \theta_o)(\sin \theta \sin \theta_s \cos(\phi - \phi_s) + \cos \theta \cos \theta_s). \quad (45)$$

In the current study, we only consider the tidally locked configuration, which is likely to be relevant for the current crop of hot Jupiters as well as temperate planets orbiting low-mass stars. In this case, the sub-stellar location is equatorial, $\theta_s = \pi/2$, $\theta_o = i$, and one can place the prime meridian at the sub-stellar meridian with no loss of generality ($\phi_s = 0$): $\pi K_{nz}(\theta, \phi, t) = \sin i \sin^2 \theta \cos \phi \cos(\phi - \phi_o) + \cos i \sin \theta \cos \theta \cos \phi$.

If the planet also orbits edge-on, $\phi_s = 0$, then: $\pi K_{nz}(\theta, \phi, t) = \sin^2 \theta \cos \phi \cos(\phi - \phi_o)$.

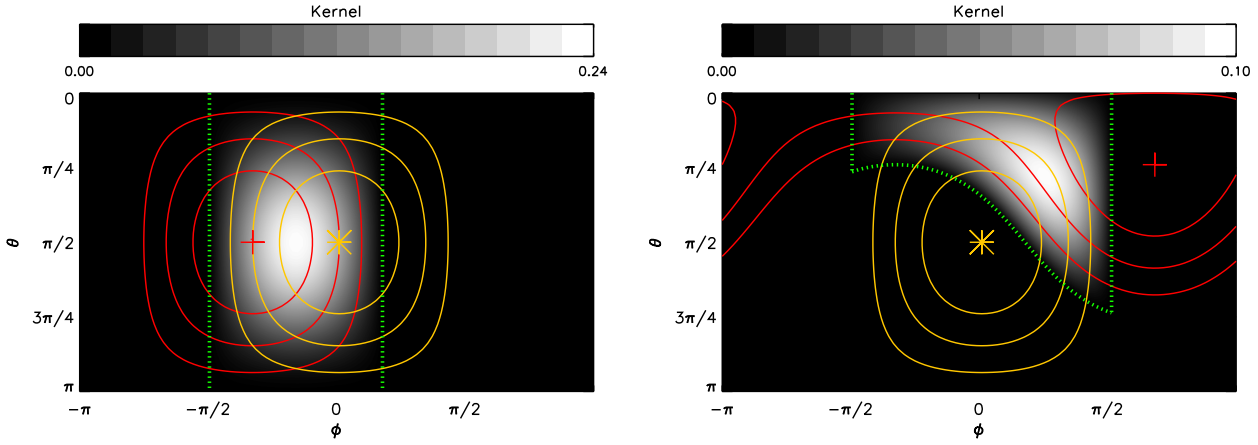


Figure 4. The visibility (red contours) and illumination (yellow contours) of a tidally-locked planet seen by an equatorial (left) and northern (right) observer. The limb and terminator are shown in each case with green dotted lines. The sub-observer location is denoted by a red cross, the sub-stellar location by a yellow asterisk. The limb and terminator are both great circles, making the non-zero portion of the kernel a lune. The maximum value of the kernel, and its integral, are a function of the angular distance between the sub-observer and sub-stellar locations, i.e.: the planet’s orbital phase.

4.2 Tidally-Locked, Edge-On Reflected Lightcurve

The combination of tidally-locked rotation and edge-on orbit dictates that the θ -integral runs from 0 to π , so the double integral can be split into two single integrals:

$$F_l^m(t) = \frac{N_l^m}{\pi} \int_{-1}^1 (1-x^2) P_{lm}(x) dx \int_{\phi_1}^{\phi_2} \cos \phi \cos(\phi - \phi_o) \cos(m\phi) d\phi, \quad (46)$$

where $\phi_1 = \max[-\pi/2, \phi_o - \pi/2]$, and $\phi_2 = \min[\pi/2, \phi_o + \pi/2]$ (left panel of Figure 4), and we have again shown the cosine case. The x -integral is merely a scalar, so $F_l^m \propto F_\lambda^\mu$, as for the edge-on thermal case. The time-dependence cannot be factored out of the ϕ -integral, however, so the negative and positive m lightcurves are not trivially related by the substitution $\cos(m\phi) \rightarrow \sin(|m|\phi)$ (cf. the $m = -1$ and $m = 1$ cases of Equation 47).

As with the edge-on thermal lightcurve, the integral over x may be solved for arbitrary l and m by using recurrence relations for Associated Legendre Polynomials and the Jepsen et al. (1955) solution to their definite integral. In the present case, this leads to terribly cumbersome expressions, so we instead adopt the brute force approach of analytically integrating the x -integral for specific l and m .

The ϕ -integral must be solved separately in two cases: $\phi_o < 0$ and $\phi_o \geq 0$ for the first and second halves of the planet’s orbit, respectively. The two cases may be stitched together by noting that $\alpha = |\phi_o|$:

$$\int_{\phi_1}^{\phi_2} \dots d\phi = \begin{cases} \frac{-\sin(m\phi_o/2)}{m(m^2-4)} \left((m+2) \sin\left(\alpha - \frac{m\alpha}{2} + \frac{m\pi}{2}\right) + (m-2) \sin\left(\alpha + \frac{m\alpha}{2} - \frac{m\pi}{2}\right) \right) & \text{if } m < -2 \\ \frac{1}{4} \sin \phi_o (\pi - \alpha + \sin \alpha \cos \alpha) & \text{if } m = -2 \\ \frac{1}{3} \sin \phi_o (1 + \cos \alpha) & \text{if } m = -1 \\ \frac{1}{2} (\sin \alpha + (\pi - \alpha) \cos \alpha) & \text{if } m = 0 \\ \frac{4}{3} \cos^4(\phi_o/2) & \text{if } m = 1 \\ \frac{1}{4} \cos \phi_o (\pi - \alpha + \sin \alpha \cos \alpha) & \text{if } m = 2 \\ \frac{\cos(m\phi_o/2)}{m(m^2-4)} \left((m+2) \sin\left(\alpha - \frac{m\alpha}{2} + \frac{m\pi}{2}\right) + (m-2) \sin\left(\alpha + \frac{m\alpha}{2} - \frac{m\pi}{2}\right) \right) & \text{if } m > 2. \end{cases} \quad (47)$$

The first few non-zero harmonic lightcurves are:

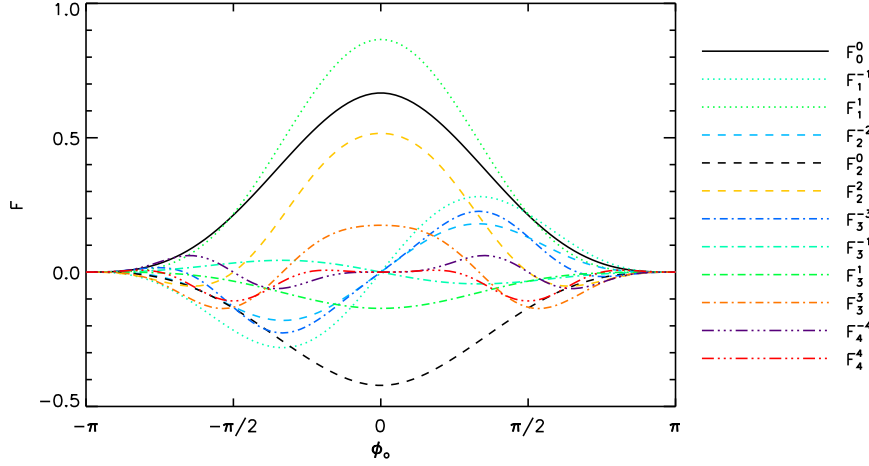


Figure 5. Harmonic reflected lightcurves for a tidally-locked planet on an edge-on orbit. Line style denotes l , color denotes m .

$$F_0^0(t) = \frac{2}{3\pi} (\sin \alpha + (\pi - \alpha) \cos \alpha) \quad (48)$$

$$F_1^{-1}(t) = \frac{\sqrt{3}}{8} \sin \phi_o (1 + \cos \phi_o) \quad (49)$$

$$F_1^1(t) = \frac{\sqrt{3}}{2} \cos^4(\phi_o/2) \quad (50)$$

$$F_2^{-2}(t) = \frac{\sin \phi_o}{\pi\sqrt{15}} ((\pi - \alpha) + \cos \alpha \sin \alpha) \quad (51)$$

$$F_2^0(t) = \frac{-2}{3\pi} \sqrt{\frac{2}{5}} (\sin \alpha + (\pi - \alpha) \cos \alpha) \quad (52)$$

$$F_2^2(t) = \frac{2 \cos \phi_o}{\pi\sqrt{15}} ((\pi - \alpha) + \cos \alpha \sin \alpha) \quad (53)$$

$$F_3^{-3}(t) = \frac{1}{192} \sqrt{\frac{35}{2}} (6 \sin \phi_o + 5 \sin(2\phi_o) - \sin(4\phi_o)) \quad (54)$$

$$F_3^{-1}(t) = \frac{-1}{32} \sqrt{\frac{7}{6}} \sin \phi_o (1 + \cos \phi_o) \quad (55)$$

$$F_3^1(t) = \frac{-1}{8} \sqrt{\frac{7}{6}} \cos^4(\phi_o/2) \quad (56)$$

$$F_3^3(t) = \frac{1}{192} \sqrt{\frac{35}{2}} (4 \cos \phi_o + 5 \cos(2\phi_o) - \cos(4\phi_o)) \quad (57)$$

$$F_4^{-4}(t) = \frac{4}{\pi\sqrt{35}} \frac{\sin^5 \alpha \cos \alpha}{\sin \phi_o} \quad (58)$$

$$F_4^4(t) = \frac{2}{\pi\sqrt{35}} \sin^3 \alpha \cos(2\phi_o). \quad (59)$$

A uniform map, $M(\theta, \phi) \equiv 1$, produces the Lambert phase function, as expected. The nullspace of the convolution includes odd $l + m$ (equivalently, odd $l - m$; i.e., an odd number of nodes in the meridional direction), for which the contribution from the northern and southern hemispheres cancel perfectly. Unlike the edge-on thermal case, and counter-intuitively, purely meridional maps, such as $Y_2^0(\theta, \phi)$, are not in the nullspace.

The harmonic lightcurves are shown in Figure 5. As expected, the negative and positive m are not related by a simple phase shift. Significantly, harmonic lightcurves with the same m are proportional to each other. Therefore, although the nullspace of this convolution is more limited than for thermal lightcurves, there are still severe formal degeneracies in the inverse problem.

4.3 Tidally-Locked, Inclined Reflected Lightcurve

In the more general case of a tidally-locked planet on an inclined orbit, the expression for harmonic lightcurves becomes:

$$F_l^m(t) = \frac{N_l^m}{\pi} \left\{ \sin i \int_{-\pi/2}^{\pi/2} \cos \phi \cos(\phi - \phi_o) e^{im\phi} \left[\int_{x_{\text{limb}}}^1 (1 - x^2) P_{lm}(x) dx \right] d\phi \right. \\ \left. + \cos i \int_{-\pi/2}^{\pi/2} \cos \phi e^{im\phi} \left[\int_{x_{\text{limb}}}^1 x \sqrt{1 - x^2} P_{lm}(x) dx \right] d\phi \right\}, \quad (60)$$

where x_{limb} is given by (28) and the meridional limits of integration implicitly assume a northern observer (right panel of Figure 4). For a southern observer the limits would be $[-1, x_{\text{limb}}]$. The limits of integration for the ϕ -integral no longer span 2π radians and therefore do not lend themselves to the Fourier strategy used for the inclined thermal lightcurves.³ Instead, we solve the integrals numerically and plot the solutions in Figure 6.

³ Moreover, the locations of the jumps in the integrand of the ϕ -integral are not as predictable as they are in the inclined thermal lightcurve case.

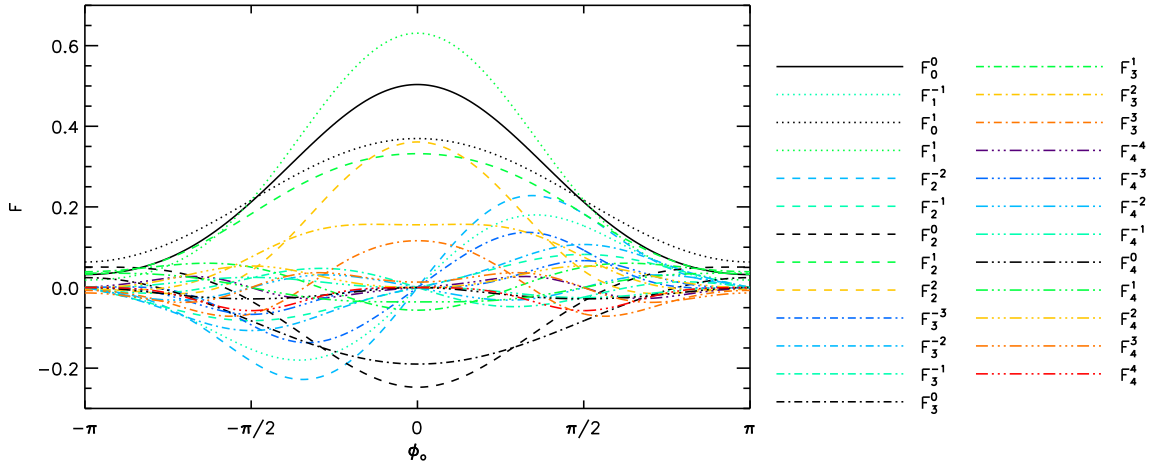


Figure 6. Harmonic reflected lightcurves for a tidally locked planet on an inclined orbit ($i = \theta_o = \frac{\pi}{4}$). Line style denotes l , color denotes m .

From numerical integration, we determine that there is no nullspace for the inclined reflected lightcurves up to $l = 4$, nor do the lightcurves depend simply on θ_o . In other words, one cannot simply scale the edge-on solutions of Figure 5 by $\sin i$. For example, the shape of F_2^0 remains fixed but with the addition of a constant offset. This means that the Y_2^0 component of the map has the effect of decreasing the reflectance of the planet at full phase and increasing it at crescent phases. This is essentially a restatement of the latitude-albedo effect noted by Cowan et al. (2012b): reflective poles make a low-obliquity planet appear abnormally bright at crescent phases.

5 DISCUSSION

5.1 Thermal Phase Variations of Short Period Planets

It is significant that there are different nullspaces for the edge-on and inclined thermal lightcurves. One can't simply scale the edge-on solution of Cowan & Agol (2008) by $\sin i$. For transiting systems, the orbital inclination is nearly 90° and is well measured by the transit morphology (e.g., Charbonneau et al. 2000). This means that while the amplitude of odd modes in an observed thermal lightcurve is likely an order of magnitude weaker than for adjacent even modes, a measurement of these modes could be readily converted into an estimate of the N-S asymmetry of the planet.

Moreover, the amplitude of odd modes in the observed lightcurve of a non-transiting planet provides a qualitative estimate of orbital inclination, since the planet may be assumed to have zero-obliquity. The original motivation for measuring thermal phase variations of hot Jupiters was to estimate orbital inclination in order to break the $M \sin i$ degeneracy (Agol & Charbonneau 2005). That proposal was based on the presumption that all hot Jupiters would have the same day-night temperature contrast ($m = 1$ amplitude). While that assumption is demonstrably wrong (Cowan et al. 2007), the inclination-dependence of thermal phase variation Fourier spectra offers an opportunity to constrain orbital inclination after all.

The best-characterized hot Jupiter, HD 189733b, only has empirical constraints up to $m = l = 2$ at 3.6 and 4.5 micron (Knutson et al. 2012). The amplitude of the $m = 2$ component of the phase variations is 5% of that at $m = 1$ for both wavebands, indicating that the $m = 2$ map has only 12% the amplitude of the $m = 1$ map (following Cowan & Agol 2008). This is not surprising since diurnal forcing primarily excites the $m = 1$ mode. The 8 micron 2D map of HD 189733b only constrains lightcurves to $l = 1$ (Majeau et al. 2012), so the strength of $m < l$ modes, in particular the N-S asymmetry responsible for odd lightcurve modes, is currently unknown empirically (and debated theoretically: Cho et al. 2003; Cooper & Showman 2005). Aside from the intrinsically weak signal, possible complications include limb-darkening, which slightly modifies the convolution kernel (Cowan & Agol 2008), the presence of eccentricity seasons (Lewis et al. 2013), or the contamination of $m = 2$ modes by ellipsoidal variations (Cowan et al. 2012a).

5.2 Rotational Modulation of Stars and Brown Dwarfs

Likewise, the Fourier spectra of spotty stars (Lanza et al. 2009) and brown dwarfs (Artigau et al. 2009; Radigan et al. 2012) might hint at their rotational inclination. This is unsurprising given that star spot modeling can yield inclination estimates good to tens of degrees (Walker et al. 2007). However, aside from being faster than traditional spot modeling, our Fourier approach suggests *why* star spot modeling is able to constrain inclination despite the myriad degeneracies (Dorren 1987; Kipping 2012). It should be feasible, by the same token, to measure the presence of odd modes in Spitzer Space Telescope lightcurves of spotty brown dwarfs to obtain a qualitative measurement of their inclination.

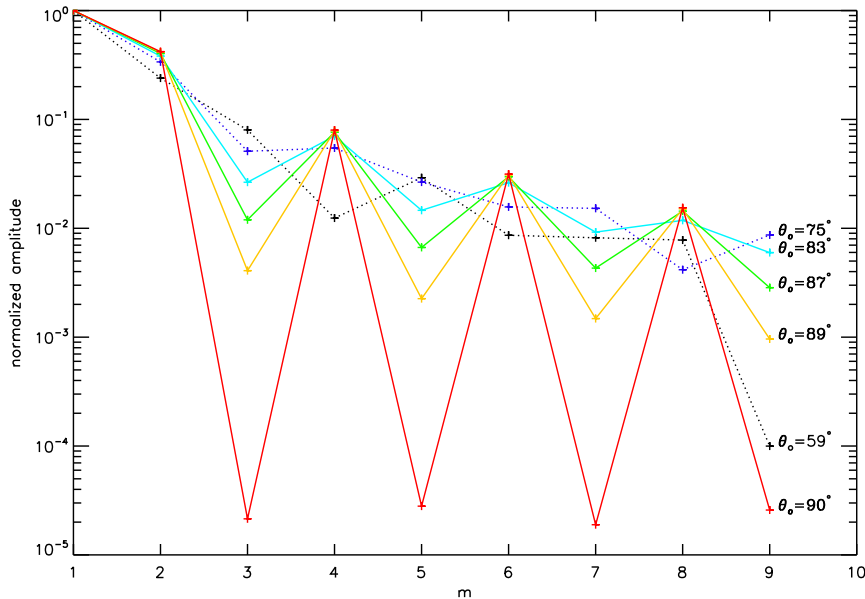


Figure 7. Fourier spectrum for a star of unit intensity with a square spot of size $\pi/10$, zero intensity, and centered on $\theta = \pi/3$, $\phi = \pi/3$. Each color corresponds to the power spectrum as measured by an observer at a different inclination. The spectra have been normalized to their $m = 1$ amplitude. An edge-on rotation produces no power in the odd modes (the non-zero values on the plot are due to numerical errors). The plot looks qualitatively similar for different spot sizes and locations, provided the spot is not equatorial, which kills $m \neq l$ modes in the map, and hence odd modes in the lightcurve.

The stellar/brown dwarf inclination inverse problem is more favorable than extracting the orbital inclination of hot Jupiters because the signal-to-noise ratio for the variations are much greater ($\sim 1\%$ rather than $\sim 0.1\%$), and the intrinsic power spectrum of the thermal map does not drop precipitously with m . The limiting case of a single δ -function spot has a flat Fourier spectrum. This makes Fourier analysis an inefficient means of mapping star spots, but potentially useful for constraining rotational inclination. Lumme et al. (1990) used the power spectra of reflected lightcurves to extract the rotational orientation of asteroids, independent of shape and albedo markings. Our work extends this approach to thermal lightcurves.

In Figure 7 we show the power spectra for a rotating star at different inclinations. For stars that are rotating nearly edge-on ($\theta_o = 90\text{--}80^\circ$, denoted by solid lines) the power at odd m is a very strong function of orientation. If one reasonably assumes that a star’s intrinsic intensity map should not be deficient in odd modes, then a factor-of-two measurement of odd amplitudes constrains the rotational inclination to within a degree. While the *a priori* odds of a star being within 10° of edge-on are not great, they increase substantially for stars known to host transiting planets (Sanchis-Ojeda et al. 2012). At larger inclinations (denoted by dotted lines), the orientation of the star still leaves an imprint on its Fourier spectrum, but one would need a strong prior on the intrinsic power spectrum of the stellar intensity map. It is not clear whether a Fourier approach would be advantageous to the usual star spot modeling in such a case.

Fourier analysis of rotating inhomogeneous bodies is analogous —conceptually and mathematically— to estimating stellar inclinations with asteroseismology (Gizon & Solanki 2003). Although our proposed method requires high-precision photometry, the observational cadence could be considerably lower than for asteroseismology, so many *Kepler* target stars may be amenable to such an analysis, without the need for $v \sin i$ measurements from high-resolution stellar spectra (e.g., Hirano et al. 2012). As with any star-spot based inclination estimate, problems include differential rotation of star spots, or their formation/dissipation on rotational timescales. If the brightness markings evolve on timescales longer than the rotational period, it should still be possible to Fourier decompose each rotation separately to perform the spectral power analysis. Limb-darkening is again a source of systematic uncertainty/error. The intrinsic power in the Y_4^3 map will depend on the latitude of star-spots, with equatorial spots providing no power at this harmonic. But star spots are, if anything, less likely to be at the equator (Baumann et al. 2004). It is not known whether the clear/cloudy regions on L/T transition dwarfs have preferred latitudes.

5.3 Obliquity of Directly-Imaged Planets

Directly imaged jovian planets emit thermal radiation because they are still young. Although no rotational variability has yet been reported for these objects, they are probably cloudy (e.g., Madhusudhan et al. 2011) and may exhibit the same sort of variability as brown dwarfs. Merely detecting this rotational modulation would be a technical feat with important implications for giant planet formation. Further down the road, however, we might hope to measure their rotational lightcurves with sufficient precision to constrain their rotational inclination with respect to our line of sight. Unlike hot Jupiters, directly

imaged Jovian planets are not tidally locked, but their orbital inclination may be estimated observationally. The Fourier spectrum of such a rotational lightcurve would therefore put a joint constraint on the planet's obliquity and equinox via:

$$\cos \theta_o = \sin \Theta \cos \xi_\Theta \sin i + \cos \Theta \cos i, \quad (61)$$

where Θ is the planetary obliquity and ξ_Θ is the angular location of northern summer solstice with respect to superior conjunction.

This is not the only method that has been proposed to measure the obliquity of directly-imaged planets. Full-orbit thermal phase curves of mature planets, for which insolation rather than internal heat dominates the power budget, might in principle betray the obliquity of a planet, but the inverse problem is complicated by orbital eccentricity, diurnal heating, and the details of heat storage and transport (Gaidos & Williams 2004; Cowan et al. 2012c). Reflected full-orbit lightcurves of directly-imaged planets have also been demonstrated to convey information about planetary obliquity (Fujii & Kawahara 2012). These methods have the advantage that they can break the degeneracy between obliquity and its orientation, but they require observations spanning the planetary orbit rather than its rotation, and therefore may not be practical for long-period planets.

5.4 Reflected Phase Variations of Planets

The fact that $F_2^0 \propto F_0^0$ for edge-on reflected phase curves has important implications for the retrieval of albedo from planetary phase variations. The Y_2^0 map corresponds to a zonally uniform planet with bright poles and has the effect of reducing the amplitude of zeroth-order (Lambertian) phase variations. Consider the worst-case of a diffusely-reflecting planet with albedo map $M = \frac{1}{3}Y_0^0 + \frac{2}{3\sqrt{10}}Y_2^0$, which has an albedo of unity at both poles, zero at the equator, and a mean albedo of $\langle M \rangle = \frac{1}{3}$ (this is qualitatively similar to the albedo map of a low-obliquity planet with polar snow/ice). The Bond albedo of the planet is $A = \frac{1}{3}A_0^0 + \frac{2}{3\sqrt{10}}A_2^0 = \frac{1}{4}$ (Appendix C). The reflected lightcurve for the planet, however, is $F(t) = \frac{1}{3}F_0^0(t) + \frac{2}{3\sqrt{10}}F_2^0(t) = \frac{1}{5}F_0^0(t)$. In other words, an observer would see a planet exhibiting perfectly Lambertian phase variations and would infer a planetary albedo of 20%. The sub-observer and sub-stellar latitudes are both equatorial, but the albedo estimate differs from the actual Bond albedo by $0.05/0.20 = 25\%$ (and differs from the mean albedo by 67%). One should therefore be wary of estimating an exoplanet's Bond albedo, even if the planet orbits edge-on, is tidally locked, and exhibits Lambertian phase variations. Precision is no guarantee of accuracy.

The inclined tidally-locked reflected lightcurves exhibit no nullspace up to $l = 4$, but the non-orthogonality of harmonic lightcurves leads to formal degeneracies for mapping planets, even in the limit of noiseless data. It remains to be seen to what extent such degeneracies affect the spin-orbit exo-cartography of Fujii & Kawahara (2012). Although we have only derived reflected lightcurves for tidally-locked planets, our results regarding meridional albedo markings affecting reflected phase variations should apply for non-locked planets, provided one averages over the rotational variation, as well as non-zero obliquity (e.g., the numerical simulations of Cowan et al. 2012b).

By deriving the reflected lightcurves exhibited by spherical harmonic maps, Russell (1906) demonstrated the existence of a nullspace for albedo markings on a distant body viewed at opposition: the odd harmonics. Researchers have dealt with this formal degeneracy by imposing positivity of albedo at every location on the body, adopting a limited number of discrete spots (Marcialis 1988), and/or using only two albedo values (light and dark regions; Lacis & Fix 1972). In this paper we have shown that such degeneracies are generically present in exo-cartographic inverse problems. We have not attempted to resolve these degeneracies, since the specific strategies involved will likely depend on the application. The silver lining is that the inclination-dependence of the convolution may provide leverage for constraining the viewing geometry of unresolved systems.

ACKNOWLEDGMENTS

NBC thanks J.H. Steffen and W.M. Farr for useful Mathematica tips. HMH was supported by an NSF postdoctoral fellowship.

REFERENCES

- Agol, E., & Charbonneau, D. 2005, Spitzer Proposal, 20482
 Artigau, É., Bouchard, S., Doyon, R., & Lafrenière, D. 2009, ApJ, 701, 1534
 Aster, R.C., Borchers, B. and Thurber, C.H., 2013, Parameter Estimation And Inverse Problems (Elsevier Academic Press)
 Baumann, I., Schmitt, D., Schüssler, M., & Solanki, S. K. 2004, A&A, 426, 1075
 Charbonneau, D., Brown, T. M., Latham, D. W., & Mayor, M. 2000, ApJ, 529, L45
 Cho, J. Y.-K., Menou, K., Hansen, B. M. S., & Seager, S. 2003, ApJ, 587, L117
 Cooper, C. S., & Showman, A. P. 2005, ApJ, 629, L45
 Cowan, N. B., Agol, E., & Charbonneau, D. 2007, MNRAS, 379, 641
 Cowan, N. B., & Agol, E. 2008, ApJ, 678, L129
 Cowan, N. B., Agol, E., Meadows, V. S., et al. 2009, ApJ, 700, 915
 Cowan, N. B., Robinson, T., Livengood, T. A., et al. 2011, ApJ, 731, 76
 Cowan, N. B., Machalek, P., Croll, B., et al. 2012, ApJ, 747, 82

- Cowan, N. B., Abbot, D. S., & Voigt, A. 2012, ApJ, 752, L3
 Cowan, N. B., Voigt, A., & Abbot, D. S. 2012, ApJ, 757, 80
 Cowan, N. B., & Strait, T. E. 2013, ApJ, 765, L17
 DiDonato, A.R. 1982, Mathematics of Computation, 38, 547
 Dorren, J. D. 1987, ApJ, 320, 756
 Fujii, Y., Kawahara, H., Suto, Y., et al. 2011, ApJ, 738, 184
 Fujii, Y., & Kawahara, H. 2012, ApJ, 755, 101
 Gaidos, E., & Williams, D. M. 2004, New Astronomy, 10, 67
 Gizon, L., & Solanki, S. K. 2003, ApJ, 589, 1009
 Hasinoff, S.W., Levin, A., Goode, P.R., Freeman, W.T., 2011 IEEE Internat. Conf. on Computer Vision (ICCV), 185
 Hirano, T., Sanchis-Ojeda, R., Takeda, Y., et al. 2012, ApJ, 756, 66
 Jepsen, D.W., Haugh, E.F. & Hirschfelder, J.O. 1955, Proc Natl Acad Sci, 41(9), 645-7
 Kawahara, H., & Fujii, Y. 2010, ApJ, 720, 1333
 Kawahara, H., & Fujii, Y. 2011, ApJ, 739, L62
 Kipping, D. M. 2012, MNRAS, 427, 2487
 Knutson, H. A., Charbonneau, D., Allen, L. E., et al. 2007, Nature, 447, 183
 Knutson, H. A., Lewis, N., Fortney, J. J., et al. 2012, ApJ, 754, 22
 Lacis, A. A., & Fix, J. D. 1972, ApJ, 174, 449
 Lanza, A. F., Pagano, I., Leto, G., et al. 2009, A&A, 493, 193
 Lewis, N. K., Knutson, H. A., Showman, A. P., et al. 2013, ApJ, 766, 95
 Lumme, K., Karttunen, H., & Bowell, E. 1990, A&A, 229, 228
 Madhusudhan, N., Burrows, A., & Currie, T. 2011, ApJ, 737, 34
 Madhusudhan, N., & Burrows, A. 2012, ApJ, 747, 25
 Majeau, C., Agol, E., & Cowan, N. B. 2012, ApJ, 747, L20
 Marcialis, R. L. 1988, AJ, 95, 941
 Oakley, P. H. H., & Cash, W. 2009, ApJ, 700, 1428
 Radigan, J., Jayawardhana, R., Lafrenière, D., et al. 2012, ApJ, 750, 105
 Robinson, T. D., Meadows, V. S., & Crisp, D. 2010, ApJ, 721, L67
 Russell, H. N. 1906, ApJ, 24, 1
 Russell, H. N. 1916, ApJ, 43, 173
 Sanchis-Ojeda, R., Fabrycky, D. C., Winn, J. N., et al. 2012, Nature, 487, 449
 Tremaine, S. 1991, Icarus, 89, 85
 Tousey, R. 1957, Journal of the Optical Society of America (1917–1983), 47, 261
 Walker, G. A. H., Croll, B., Kuschnig, R., et al. 2007, ApJ, 659, 1611
 Wild, W. J. 1991, ApJ, 368, 622
 Williams, D. M., & Gaidos, E. 2008, Icarus, 195, 927
 Winn, J. N., Noyes, R. W., Holman, M. J., et al. 2005, ApJ, 631, 1215
 de Wit, J., Gillon, M., Demory, B.-O., & Seager, S. 2012, A&A, 548, A128

APPENDIX A: INTEGRALS OF ASSOCIATED LEGENDRE POLYNOMIALS

A technical crux of the analytic forward problem is solving definite integrals of Associated Legendre Polynomials, P_{lm} .

A1 Recurrence Relation

Recurrence relations allow us to relate functions of x including Associated Legendre Polynomials to combinations of simple Associated Legendre Polynomials. For example, we used

$$\sqrt{1-x^2}P_{lm} = \frac{-1}{2l+1} [P_{l-1,m+1} - P_{l+1,m+1}]. \quad (\text{A1})$$

A2 Definite Integrals on $x \in [-1, 1]$

For the special cases where the limits of integration are $x \in [-1, 1]$ (edge-on, zero-obliquity reflected light; equator-on thermal emission), compact solutions (i.e., not involving sums) have been worked out by Jepsen et al. (1955). Those authors solved the definite integral of $P_{lm}(x)$ without the Condon-Shortley phase, precisely what we need in the current paper:

$$R_l^m \equiv \int_{-1}^1 P_{lm}(x) dx = \begin{cases} R_l^m(\text{even}) \equiv \frac{2m[(l/2)!]^2 (l+m)!}{l![(l-m)/2]![(l+m)/2]!(l+1)!} & \text{if } l \text{ and } m \text{ are even} \\ R_l^m(\text{odd}) \equiv -\frac{\pi m (l+m)! (l+1)!}{l^{2l+1} \{[(l+1)/2]!\}^2 [(l-m)/2]! [(l+m)/2]!} & \text{if } l \text{ and } m \text{ are odd} \\ 0 & \text{if } l+m \text{ is odd,} \end{cases} \quad (\text{A2})$$

Physically, the northern and southern hemispheres have perfectly canceling lightcurves in the third case.

APPENDIX B: WHY THERMAL HARMONIC LIGHT CURVES ARE ZERO FOR ODD $l > 1$

The heart of this claim is the recognition that the calculation of (29) and (30) is formally equivalent to identifying the Fourier coefficients of the x -integral. These Fourier coefficients will vanish unless the integral of the Legendre polynomial contains a term that has a periodicity that matches the term being pulled out by the Fourier integration, i.e. a term like $\cos m\Phi$ with the correct periodicity. We argue that this never happens for odd $l > 1$ (in fact, $A = 0$ for $l = 1$ also).

First consider our expression for x_{limb} ,

$$x_{\text{limb}} = \frac{-\tan \theta_o \cos \Phi}{\sqrt{1 + \tan^2 \theta_o \cos^2 \Phi}}. \quad (\text{B1})$$

As long as $\tan \theta_o < 1$ (i.e. $\theta_o < \pi/4$) we can Taylor expand the denominator to obtain a power series in $\cos \Phi$,

$$x_{\text{limb}} = -\tan \theta_o \cos \Phi \left(1 - \frac{1}{2} \tan^2 \theta_o \cos^2 \Phi + \frac{3}{8} \tan^4 \theta_o \cos^4 \Phi + \dots \right). \quad (\text{B2})$$

Note that the power series within parentheses only contains even powers of $\cos \Phi$, and so when you multiply by the sole external term you obtain a power series containing only odd powers of $\cos \Phi$. Let's consider what this means for powers of x_{limb} and one other function of it.

The series associated to x_{limb}^2 can be found by multiplying the two series for x_{limb} and because each term is an odd power of $\cos \Phi$ the product of two such terms will be an even power of $\cos \Phi$; thus the series for x_{limb}^2 and all other even powers of x_{limb} is completely made up of even powers of $\cos \Phi$. Similarly the series for x_{limb}^3 and all odd powers of x_{limb} are completely made up of odd powers of $\cos \Phi$. Finally, note that

$$\sqrt{1 - x_{\text{limb}}^2} = \frac{1}{\sqrt{1 + \tan^2 \theta_o \cos^2 \Phi}} = \left(1 - \frac{1}{2} \tan^2 \theta_o \cos^2 \Phi + \frac{3}{8} \tan^4 \theta_o \cos^4 \Phi + \dots \right), \quad (\text{B3})$$

which is a completely even series in $\cos \Phi$. Any power of this function will also be an even series in $\cos \Phi$.

Any odd power of $\cos \Phi$ can be expanded to obtain a series in terms of $\cos m\Phi$ where m is necessarily odd, and similarly for even powers except that m is necessarily even and a constant term can also appear.

To complete the argument the specific observations above have to be combined with several general observations about the associated Legendre polynomials. Below we will frequently encounter expressions containing $(1 - x^2)^{m/2}$, which after Taylor expansion give an even power series in x . For this reason we will call these terms even, although it only applies after the expansion has been performed. From the Rodrigues' formula,

$$P_{lm}(x) = \frac{(1 - x^2)^{m/2}}{2^l l!} \frac{d^{m+l}}{dx^{m+l}} \left([x^2 - 1]^l \right), \quad (\text{B4})$$

it follows that if $l + m$ is even then the Legendre polynomial is an even power series in x . On the other hand, if $l + m$ is odd then it is an odd power series in x . These basic observations about the associated Legendre polynomials are also valid for their indefinite integrals, the proof of which follows from the results of DiDonato (1982). Applying DiDonato's results we find that for the integral

$$\int \sqrt{1 - x^2} P_{lm}(x) dx, \quad (\text{B5})$$

if $l + m$ is even the result of the integration is an odd power series in x and vice versa. While for the integral,

$$\int x P_{lm}(x) dx, \quad (\text{B6})$$

if $l + m$ is even the result of the integration is an even power series in x and if it is odd then the result is an odd power series in x . (Note that for even l these integrals also give rise to arcsine functions and these must also be Taylor expanded for the statements to be valid.)

If we adopt the complex exponential notation, the integrals of interest for the thermal light curves are

$$A_l^m(\theta_o) = \int_0^{2\pi} \cos \Phi e^{im\Phi} \int_{x_{\text{limb}}}^1 \sqrt{1 - x^2} P_{lm}(x) dx d\Phi \quad (\text{B7})$$

and

$$B_l^m(\theta_o) = \int_0^{2\pi} e^{im\Phi} \int_{x_{\text{limb}}}^1 x P_{lm}(x) dx d\Phi. \quad (\text{B8})$$

Putting aside the upper limits of the internal integrals for a moment and taking only the lower limits we can argue as follows: Focus on the A integrals first and note that for $m \geq 0$,

$$\cos \Phi e^{im\Phi} = \frac{1}{2} \left(\cos \{(m - 1)\Phi\} + \cos \{(m + 1)\Phi\} \right). \quad (\text{B9})$$

Thus viewing this as a Fourier decomposition the A integrals are the sum of the $(m - 1)$ and $(m + 1)$ coefficients. For odd l and even m , $l + m$ is odd and so the Legendre polynomial integral in A gives rise to an even power series in x , which in turn gives rise to a sum over terms of the form $\cos(nx)$ where n is either zero or even. However, in this case $(m - 1)$ and $(m + 1)$ are odd and hence the integral is zero (there are no odd terms to pick out of the series). Similarly, for odd l and odd m , $l + m$ is even and we get a power series with only odd powers of x , which in turn only give rise to odd terms in $\cos(nx)$. And in this case $(m - 1)$ and $(m + 1)$ are even and once again the integral is zero. Thus, $A_l^m = 0$ for odd $l > 1$.

Chasing the even-odd parity of l , m and $l + m$ similarly for the B integrals gives you the same result for $l > 1$, i.e. $B_l^m = 0$ for odd $l > 1$.

It is interesting to briefly comment on why these results don't apply to the case $l = 1$, and we also explain why the upper limits of integration don't contribute to the integrals considered above. For $l = 1$ and $m = 0$ the argument above does apply to the A integral while the B integral is no longer formally equivalent to a Fourier series, there is no cosine term in the outer integral, and so F_1^0 receives a contribution from the B integral. In the $l = 1, m = 1$ case, the argument above applies to the B integral but not to the A integral which after using Eq. (B9) has a contribution with no cosine term. In both these special cases the upper limit of integration contributes because it is not integrated against a cosine term which when it is present cause the integration of the constant term to die.

One final comment: the argument above started by assuming that θ_o was in the range $[0, \pi/4]$ in order that the Taylor expansion of the square-root made sense. However, the expansion can be continued to the range $[\pi/4, \pi/2]$ and the same argument run again, although the series is no longer convergent and hence is rather formal. In this manner, the conclusions about the null space for the northern observer can be carried over to the full range $\theta_o \in [0, \pi/2]$.

APPENDIX C: BOND ALBEDO OF A TIDALLY-LOCKED PLANET

The Bond-albedo for a tidally-locked planet is time-invariable:

$$A = \frac{1}{\pi} \oint A(\theta, \phi) I(\theta, \phi, t) d\Omega. \quad (\text{C1})$$

The contribution to the Bond albedo from a cosine harmonic map is

$$A_l^m = \frac{N_l^m}{\pi} \int_{-1}^1 \sqrt{1-x^2} P_{lm}(x) dx \int_{-\frac{\pi}{2}}^{\frac{\pi}{2}} \cos \phi \cos(m\phi) d\phi, \quad (\text{C2})$$

which is identical to (15) but with $\phi_o \equiv 0$. By analogy, the solution is simply

$$A_l^m = \begin{cases} 1 & \text{if } l = 0 \\ \frac{2}{\sqrt{3}} & \text{if } l = 1 \text{ and } |m| = 1 \\ \frac{2(-1)^{m/2}}{\pi(1-m^2)} \sqrt{\frac{2(l-m)!}{(2l+1)(l+m)!}} [R_{l+1}^{m+1}(\text{odd}) - R_{l-1}^{m+1}(\text{odd})] & \text{if } l \text{ and } m \text{ are even} \\ 0 & \text{otherwise,} \end{cases} \quad (\text{C3})$$

where $R_l^m(\text{odd})$ is given in Appendix B. The nullspace is the union of odd $|m| > 1$ (ϕ -integral goes to zero) and odd $l > 1$ (x -integral goes to zero).